Unstructured LES of reacting multiphase flows in realistic gas turbine combustors

By Frank Ham, Sourabh Apte, Gianluca Iaccarino, Xiaohua Wu, Marcus Herrmann, George Constantinescu†, Krishnan Mahesh‡ AND Parviz Moin

1. Motivation and objectives

As part of the Accelerated Strategic Computing Initiative (ASCI) program, an accurate and robust simulation tool is being developed to perform high-fidelity LES studies of multiphase, multiscale turbulent reacting flows in aircraft gas turbine combustor configurations using hybrid unstructured grids. In the combustor, pressurized gas from the upstream compressor is reacted with atomized liquid fuel to produce the combustion products that drive the downstream turbine. The Large Eddy Simulation (LES) approach is used to simulate the combustor because of its demonstrated superiority over RANS in predicting turbulent mixing, which is central to combustion.

CDP is the flagship LES code being developed by the combustor group to perform LES of reacting multiphase flow in complex geometry. CDP is named after the late Charles David Pierce (1969-2002) who made several lasting contributions to the LES of reacting flows and to this ASCI program. CDP is a parallel unstructured finite-volume code developed specifically for LES of variable density low Mach-number flows. It is written in Fortran 90, uses MPI, and has integrated combustion and spray modules. In the first five years of ASCI (1997-2002), the principle focus of the combustor group was the development and validation of an entirely new numerical method with the characteristics necessary for simultaneously accurate and robust LES on unstructured grids. These competing ends were both achieved by developing a method around the principle of discrete kinetic energy conservation (Mahesh *et al.* 2003). This numerical algorithm has now been extended to variable density, low-Mach number multiphase reacting flows.

In March of 2003, with the underlying numerics established and validated in a variety of flows, a major redesign and rewrite of the code was initiated. Called CDP-α, this new version of the code will have all the capabilities of the current code along with considerable improvements, all of which are considered critical to achieving the stated ASCI goal of a "major advance in engine simulation technology."

This paper summarizes the accomplishments of the combustor group over the past year, concentrating mainly on the two major milestones achieved this year:

• Large scale simulation: A major rewrite and redesign of the flagship unstructured LES code has allowed the group to perform large eddy simulations of the complete combustor geometry (all 18 injectors) with over 100 million control volumes.

• Multi-physics simulation in complex geometry: The first multi-physics simulations including fuel spray breakup, coalescence, evaporation, and combustion are now being performed in a single periodic sector ($1/18^{th}$) of an actual Pratt & Whitney combustor geometry.

† University of Iowa
‡ University of Minnesota

2. New CDP Code Development: CDP-α

In March of 2003, development of a new version of CDP, CDP-α, was initiated with the goal of performing large-scale simulation of the full Pratt & Whitney combustor. When completed, CDP=α will have all the capabilities of the existing CDP code, with the following improvements:

- Parallel preprocessing to allow unstructured simulations of 100 million control volumes or more,
- Faster, more scalable solvers based on geometric and/or algebraic multigrid methods,
- Particle/mesh load balancing capabilities,
- Integrated postprocessing capabilities, including the parallel computation and writing of plane and isosurface cuts of instantaneous or statistical data, and the seeding and tracking of massless Lagrangian particles,
- Generally improved code modularity and design, allowing users several levels of interaction with the code, and rapid implementation and testing of new models and capabilities,
- Regression testing and version control.

At the time of writing, the parallel preprocessor has been completed, and a cold flow (incompressible) version of CDP-α has been completed and verified against the old code in a variety of incompressible flow calculations. A Fortran 90 interface to the algebraic multigrid solver of LLNL's CASC group (Falgout *et al.* 2002) has been added as an option for solving the Poisson system, resulting in a significant overall speedup, although at a substantial memory overhead. Particle/mesh load balancing capabilities have been added and tested using model particle distributions. Details of these capabilities are described in the following subsections.

2.1. *Parallel Preprocessing*

CDP requires as input N_p separate grid partition files, where N_p is the number of processors that will be used for the LES. These partition files describe the grid (nodes, faces, control volumes) associated with a particular partition, and also contain the connectivity graph. The preparation of these N_p partition files is called preprocessing, and consists of four distinct steps:

- geometry definition
- grid generation
- grid partitioning
- reordering/redistribution

Up to now, the combustor group simulations have used a single-processor preprocessing strategy to generate and preprocess hybrid unstructured grids up to a maximum size of about 14 M control volumes (cv's). This is approximately the maximum size that can fit within the 8 GByte physical memory of the high-end workstation used for grid generation. At this size, the grid is extremely cumbersome to inspect for quality, and a more reasonable limit is about 5 M cv's.

To preprocess grids of order 100 M cv's, it was necessary to develop a new parallel preprocessor. Some recent aircraft simulations in the literature have used unstructured tetrahedral grids close to this size (25 to 60 M vertices) (Mavriplis & Pirzadeh 1999). These grids were generated using a two step approach. First an unstructured grid of several million vertices was generated and partitioned on a work-station. These partitions were subsequently refined using homothetic refinement on a supercomputer. This
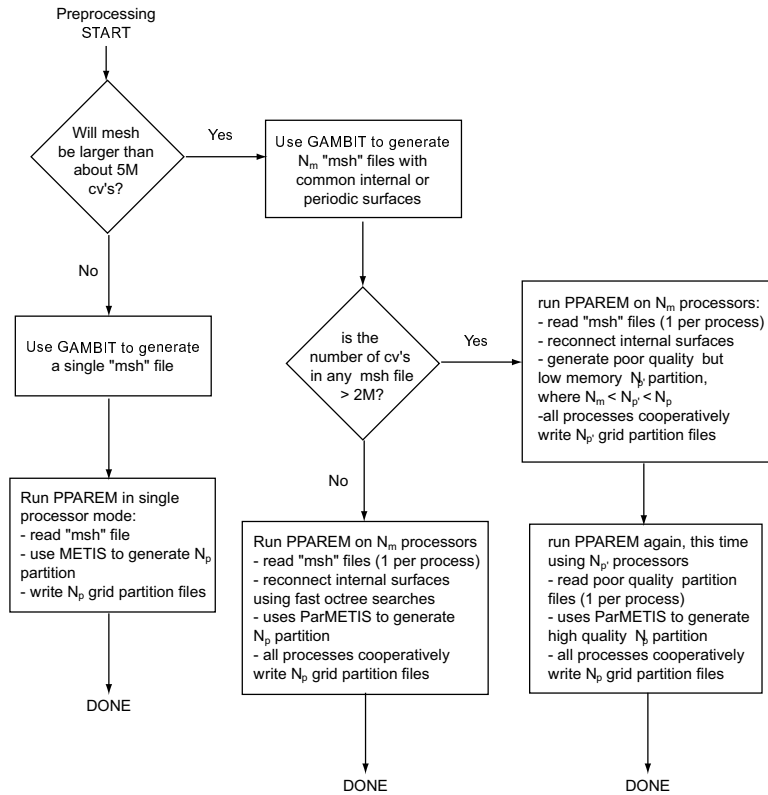
Preprocessing
START

Will mesh be larger than about 5M cv's?

Yes — Use GAMBIT to generate N_m "msh" files with common internal or periodic surfaces

No

Use GAMBIT to generate a single "msh" file

is the number of cv's in any msh file > 2M?

Yes — run PPAREM on N_m processors:
- read "msh" files (1 per process)
- reconnect internal surfaces
- generate poor quality but low memory $N_{p'}$ partition, where $N_m < N_{p'} < N_p$
- all processes cooperatively write $N_{p'}$ grid partition files

No

Run PPAREM in single processor mode:
- read "msh" file
- use METIS to generate N_p partition
- write N_p grid partition files

DONE

Run PPAREM on N_m processors
- read "msh" files (1 per process)
- reconnect internal surfaces using fast octree searches
- uses ParMETIS to generate N_p partition
- all processes cooperatively write N_p grid partition files

DONE

run PPAREM again, this time using $N_{p'}$ processors
- read poor quality partition files (1 per process)
- uses ParMETIS to generate high quality N_p partition
- all processes cooperatively write N_p grid partition files

DONE

FIGURE 1. Flowchart for the Parallel Preprocessor based on Fluent's GAMBIT software for mesh generation, and our own preprocessing program called PPAREM (Parallel PArtition and REorder Mesh).

approach significantly reduces the cost of the initial grid generation, but gives up individual element control. This approach also requires a close coupling to the problem geometry during the refinement of elements along the boundary to ensure the grid remains boundary-conforming.

The present combustor simulations contain substantially more geometric complexity than the aircraft wing-body geometries typically used for simulation. Consequently, ensuring boundary conformity during refinement presents a significant challenge. Additionally, there are many regions of the geometry where control of the final grid distribution is desired, such as the geometric details of the injectors or dilution holes. Homothetic refinement without subsequent grid smoothing can introduce step-changes in the grid spacing that may adversely affect LES accuracy. For these reasons, the present parallel preprocessor was developed based on the idea of decomposing the combustor geometry into several geometrically-separated regions, and then separately generating the desired grid in each of these regions, ensuring only that shared surfaces have identical meshes. These meshes are then reassembled on the parallel computer using fast octree searches on the common face geometry.

Figure 1 illustrates the process of mesh generation using the CDP parallel preprocessor. Grid generation is still performed on a single high-end workstation using Fluent's commercial mesh generation software, GAMBIT. For mesh sizes less than about 5 mil-

TABLE 1. Parallel preprocessing of 35 M cv grid

exact cv count	35,140,896
number of msh files, N_m	18
number of final partitions, N_p	352
I/O:	
input msh files	3.72 GB
output partition files	3.01 GB
Wall clock time:	
PPAREM on N_m processors:	
read/parse msh files	504 s
octree reconnect geometry	28 s
N_p partition (ParMETIS)	45 s
write N_p partition files	1436 s
Total wall clock time	2013 s (34 min)

lion control volumes, the preprocessing is done in an entirely serial way, much as before. For larger meshes, however, the geometric decomposition approach described earlier is used, and GAMBIT is used to generate a number of separate mesh files. Our parallel preprocessing program PPAREM (Parallel PArtition and REorder Mesh) then reads and reconnects the global mesh, produces a high-quality partition that is independent of the present geometric decomposition using ParMETIS, and reorders and cooperatively writes the partition files using the MPI-I/O routines. Cooperative writing of the partition files represented a challenging programming task, but is the only theoretically scalable way to write the final partition.

The parallel preprocessor was used to prepare two large grids on LLNL's Frost for the cold flow full combustor simulations described in the next subsection. Grid sizes were approximately 35 M and 100 M cv's respectively. Due to the memory requirement of ParMETIS (approx. 0.4 GB per million cv's out of the total requirement of 0.5 GB per million CV's for PPAREM), it was necessary in the case of the 100 M cv grid to produce an intermediate partition using a low-memory but poor quality partitioning algorithm (simply binning the cv's based on global index). PPAREM was then run a second time on a larger number of processors using this poor quality partition as input. With more memory available, a high-quality partition was then calculated using ParMETIS. An alternative and presumably faster approach would be to increase the memory per processor by using more nodes. This was tried unsuccessfully up to 6 nodes for the 100 M case (i.e. 3 processors per node), at which point the "successive partitioning" strategy described previously was adopted.

Tables 1 and 2 summarize some key indices measured during preprocessing. The most expensive and apparently least scalable component of preprocessing is the cooperative reordering and writing of the partition files using MPI-I/O. In the worst case, however, preprocessing of the 100 M cv grid with 1024 partitions required 4.5 hours.

2.2. *Large-Scale Simulation*

In the process of verification and validation of CDP-α, a variety of incompressible cold flow simulations have been performed. The largest of these have been 35 M cv and 100 M cv simulations of the full P&W combustor (all 18 injectors). Figure 2 presents a snapshot

TABLE 2. Parallel preprocessing of 100 M cv grid – 2 cases

exact cv count	100,241,208	100,241,208
number of msh files, N_m	18	18
poor quality partitions, $N_{p'}$	96	96
final partitions, N_p	512	1024
I/O:		
input msh files	14.28 GB	14.28 GB
poor quality partition files	9.65 GB	9.65 GB
final partition files	8.86 GB	8.78 GB
Wall clock time:		
1. PPAREM on N_m processors:		
read/parse msh files	1550 s	1550 s
octree reconnect geometry	75 s	75 s
poor quality partition	2 s	2 s
write poor partition files	1538 s	1538 s
2. PPAREM on $N_{p'}$ processors:		
read poor quality partition	122 s	183 s
partition (ParMETIS)	387 s	501 s
write N_p partition files	6445 s	12385 s
Total wall clock time	10121 s (2.8 h)	16236 s (4.5 h)
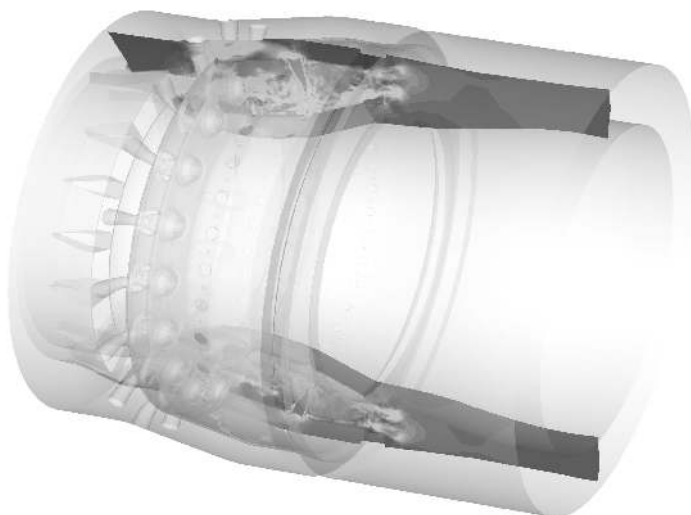
FIGURE 2. Geometry and contours of the instantaneous velocity magnitude on a plane cut through the full P&W 6000 combustor simulation, 35 M cv's.

of this simulation illustrating its substantial geometric complexity and fidelity. The maximum ratio of length scales (ratio of overall domain size to the smallest control volume sizes) is about 10^4. When the new code is completed and contains all the combustion and spray capability of the existing CDP, the ability to run such large simulations will allow the investigation of important physical phenomena, including azimuthal combustion instabilities. Their purpose at this point, however, is mainly for computer science.

2.2.1. *Multigrid*

Multigrid solvers will play an important role in achieving speed and scalability for the very large scale simulations made possible with the new code. As part of the CDP-α development, an interface was written to the hypre solvers of LLNL's CASC group (Falgout *et al.* 2002), and specifically the algebraic multigrid solver (AMG). Tests on large scale cold-flow simulations (35 M cv's on between 160 and 512 processors of Frost) where the existing preconditioned conjugate gradient solver (PCG) for pressure was replaced by AMG yielded a consistent overall speedup of over 4 times. At the largest problem size investigated of 100 M cv's, however, it was not possible to use AMG due to memory allocation errors, even when all 64 nodes of Frost were dedicated to this problem . Based on these results, the following modifications were made to the solver-related research in the combustor group:

• Although the existing CDP code will be phased out in the next few months as the combustion and spray capabilities are implemented and verified in CDP-α, the CDP-to-hypre interface was integrated into the old CDP code, where it has resulted in an overall speedup of over $2 \times$ for the multiphysics reacting flow simulations. The effect of AMG on both the old and new codes is shown in figure 3.

• The combustor group's research into geometric multigrid has been given lower priority. While the performance of geometric multigrid should theoretically be superior to the algebraic method, both methods have the property of linear scalability, and the promising results from hypre's AMG have meant that combustor group computer science resources can be concentrated on other non-scalable bottlenecks associated with CDP, including parallel preprocessing and particle/mesh load balancing.

• LLNL's CASC group has been involved to help solve the memory problems associated with the very large scale simulations, and also to provide expertise in optimizing the variety of AMG settings for our simulations.

2.2.2. *Scalability*

A scalability study of CDP-α has been performed on Frost. Figure 4 summarizes these results for the 35 M cv full combustor cold flow LES, showing acceptable scalability on up to 480 processors.

Although the full combustor simulation was also run with 100 M cv's on up to 64 nodes of Frost, this was only possible with the significantly slower PCG solver for pressure. Investigations of the code scalability at these larger problem sizes and over a greater range of processors will be made once the memory problems associated with the AMG solver have been solved.

2.2.3. *Code Performance*

Table 3 gives some of the key computer science indices for the new CDP-α code. The total memory requirement and total file size scale linearly with problem size, so these indices are reported per M cv's. We note that the AMG memory estimate is based on a number of smaller simulations made on 32 processors or fewer. Clearly such an aggregate memory requirement does not give the complete picture for large-scale simulations. Assuming linear scaling, the 100 M cv simulation should require 100 M $\times$ 3.5 GB = 350 GB, less than the physical memory available on 32 and certainly 64 nodes of Frost†. As discussed earlier, however, attempts to run the 100 M cv simulation with AMG on both 32 and 64 nodes of Frost resulted in memory allocation errors.

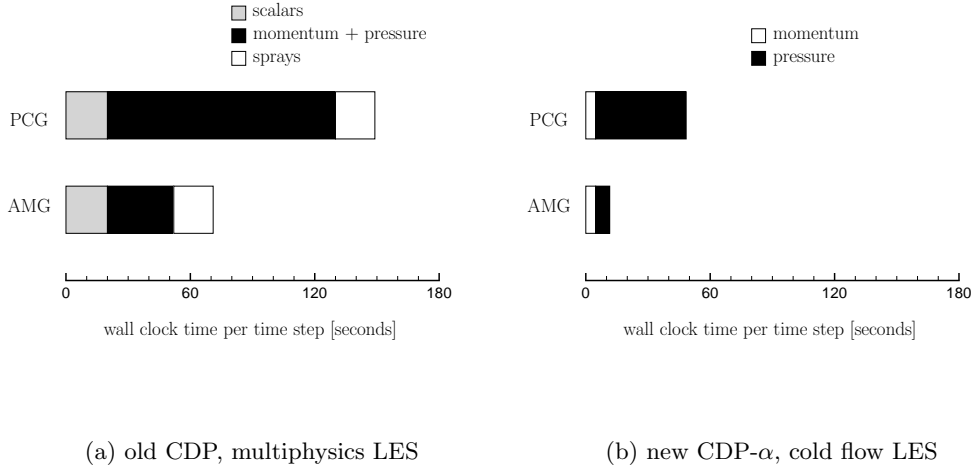† Frost has 64 nodes with 16 GB/node and 16 processors/node

(a) old CDP, multiphysics LES (b) new CDP-α, cold flow LES

FIGURE 3. Speedup of the old and new CDP codes by changing the pressure solver from pre-conditioned conjugate gradient (PCG) to hypre's algebraic multigrid (AMG): a) Old CDP code, P&W reacting flow single sector simulation with 2 M cv's on 80 processors of Frost ($\approx 25,000$ cv's/processor). b) New CDP-α, cold flow LES of full combustor, 35 M cv's on 480 processors of Frost ($\approx 73,000$ cv's/processor).
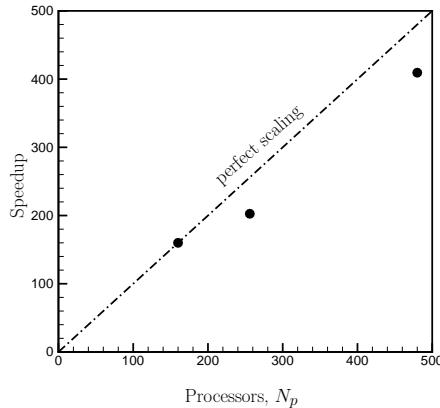

FIGURE 4. Scalability of the new CDP-α code on Frost (with hypre AMG solver for pressure). Problem is the cold flow LES of the full combustor geometry with 35 M cv's. Scaling is reported relative to the 160 processor case, which was the smallest number of Frost processors that could run this problem.

2.3. *Particle/Mesh Load Balancing*

The geometric locality of particles combined with the sequential nature of particle/mesh time advancement can create load imbalance. By integrating components of the parallel preprocessor with CDP-α, it was straight-forward to add particle/mesh load balancing capabilities to the new code. Because the code has very long run times relative to the startup time (i.e. reading the partition and restart files), we developed the load balancing strategy to work like a restart. When a threshold value of load imbalance is reached, a

TABLE 3. Some computer science indices for CDP-α

Total memory requirement	
- with PCG solver for pressure	1.5 GB per M cv's
- with AMG solver for pressure	3.5 GB per M cv's
I/O (MPI-2):	
- input partition files	0.10 GB per M cv's
- input restart or output result files	0.20 GB per M cv's
Floating point performance (Frost):	
- sustained Megaflops per processor	78.9 Mflops
- percentage of peak	5.3 %
- flops to memory references	0.294
Sample wall clock time (35 M cv on	
480 processors of Frost, cold flow):	
- startup (read partition & restart files)	13 min
- 20,000 time steps at 11 s/step	61 h
- writing result/restart files	5 min
- cooperative writing 2D plane data file	1 min

new partition is calculated using the multi-constraint option available in ParMETIS. This new partition will have (approximately) the same number of cv's and particles on each processor. This new partition is then cooperatively written to files using the routines developed for the parallel preprocessor. The simulation is then stopped, and can be restarted using the new partition.

At the time of this writing, these capabilities have been tested on small problems using model particle cost distributions only. Figure 5 illustrates a model particle cost function and an initial 32-partitioning produced by the parallel preprocessor using ParMETIS in single-constraint mode. ParMETIS was then used to repartition the problem with the dual constraints of equal numbers of cv's *and* particles on each partition. The theoretical simulation timings for the initial partition and multi-constraint partition are shown in figure 6 a) and b) respectively. Times are normalized relative to the perfectly balanced case. For this particular particle distribution, the initial partition has a normalized computation time of over 4. Using a multi-constraint repartitioning, the normalized computation time is reduced to 1.04. This implies a speedup of about 4 ×, assuming no change in parallel efficiency. The multi-constrained partitioning does, however, increase the edge cut – in this case by about 40%. The extent to which this reduces the theoretical speedup will be determined when this load balancing capability is tested on real problems.

3. Spray Models in CDP

The objective of the spray simulation effort is to develop a numerical framework based on Lagrangian particle models to perform high-fidelity LES of reacting multiphase flows encountered in realistic gas-turbine combustion chambers. Three regimes of flow development are commonly observed inside these combustors (as shown in Fig. 7): 1) 'primary breakup regime' and 'dense regime', where the liquid film exhibits large scale coherent structures that interact with the gas-phase and disintegrate into filaments by forming Kelvin-Helmholtz type instability, 2) 'intermediate regime' where the liquid blobs formed
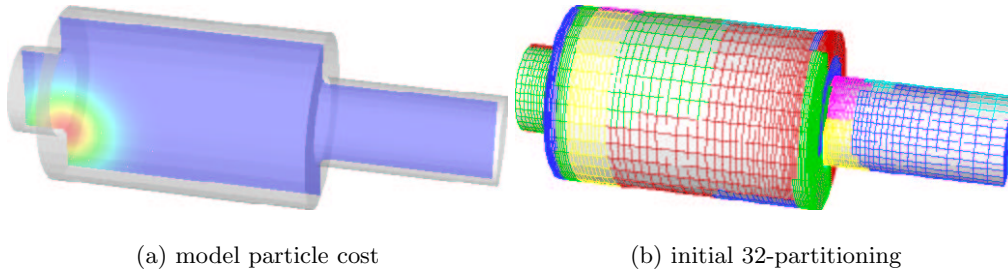
(a) model particle cost

(b) initial 32-partitioning

FIGURE 5. Sample problem used to demonstrate particle/mesh load balancing capabilities in CDP-α.

(a) single-constraint 32-partition, edge cut = 18038, normalized time = 4.05

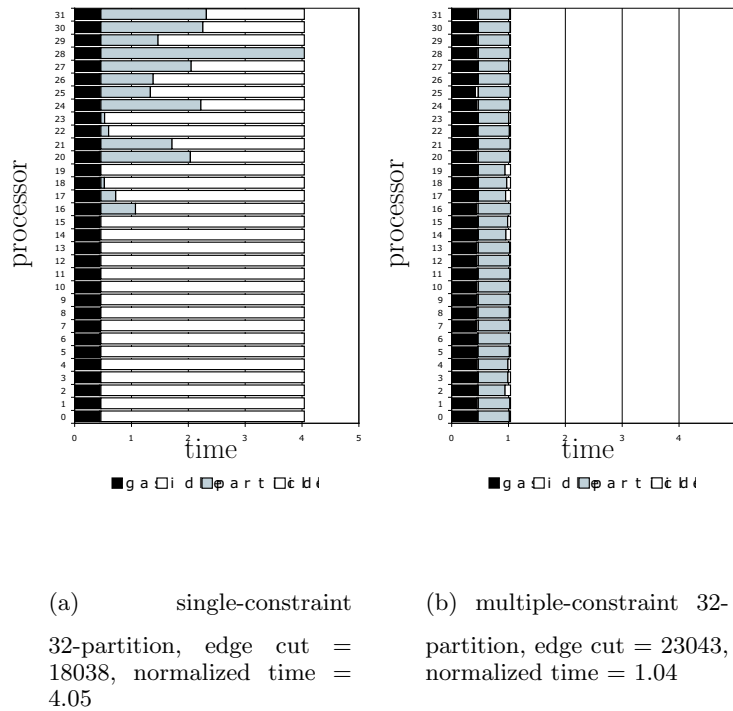(b) multiple-constraint 32-partition, edge cut = 23043, normalized time = 1.04

FIGURE 6. Computation time on each processor for sample particle/mesh load balancing problem shown in figure 5.

undergo secondary breakup, and 3) 'dilute regime' where the droplets evaporate, the fuel vapor mixes with the surrounding hot gas giving turbulent spray flames. Droplet deformation and collision are also important features in the intermediate regime. Figure 7 summarizes the characterization of the spray formation into the three regimes, based on the ratio of the characteristic length scale of the liquid to the available grid resolution $\ell/\Delta x$ and the liquid phase volume fraction Θ_p.

The main task was to integrate models capturing these complex phenomena into the unstructured LES code (CDP), perform comprehensive validation simulations of each model, and initiate large-scale turbulent, multiphase, reacting flow simulation in realistic
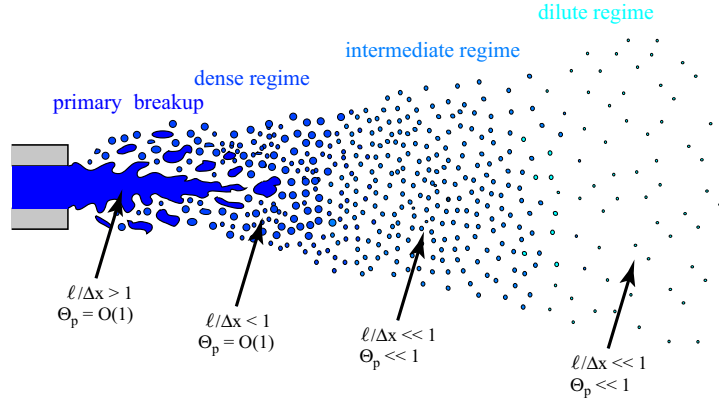
FIGURE 7. Regimes of spray formation defined by the ratio of the characteristic length scale of the liquid, ℓ, to the local grid spacing, Δx and the liquid phase volume fraction, Θ_p.

combustor geometry. A summary of Eulerian/Lagrangian equations with two-way coupling for interphase mass, momentum, and energy transport is given below. The subgrid models for sprays including secondary breakup, droplet deformation and drag, droplet evaporation, a hybrid particle-parcel approach for sprays, and accounting for finite-size effect of droplets in the dense spray regime are described in brief. Also, two novel approaches to more accurately simulate the initial 'primary breakup regime' and the 'dense regime' are briefly outlined.

3.1. *Gas-Phase Equations*

We solve the variable density, low-Mach number equations with two-way coupling between the gas-phase and liquid particles. The formulation is based on the flamelet/progress variable approach developed by Pierce & Moin (2001) for LES of non-premixed, turbulent combustion. The gas-phase continuity, scalar, and momentum equations are,

$$\frac{\partial \overline{\rho_g} \tilde{u}_j}{\partial x_j} = -\frac{\partial \overline{\rho_g}}{\partial t} + \overline{\dot{S}_m} \tag{3.1}$$

$$\frac{\partial \overline{\rho_g} \tilde{Z}}{\partial t} + \frac{\partial \overline{\rho_g} \tilde{Z} \tilde{u}_j}{\partial x_j} = \frac{\partial}{\partial x_j}(\overline{\rho_g} \tilde{\alpha}_Z \frac{\partial \tilde{Z}}{\partial x_j}) - \frac{\partial q_{Zj}}{\partial x_j} + \overline{\dot{S}_Z} \tag{3.2}$$

$$\frac{\partial \overline{\rho_g} \tilde{C}}{\partial t} + \frac{\partial \overline{\rho_g} \tilde{C} \tilde{u}_j}{\partial x_j} = \frac{\partial}{\partial x_j}(\overline{\rho_g} \tilde{\alpha}_C \frac{\partial \tilde{C}}{\partial x_j}) - \frac{\partial q_{Cj}}{\partial x_j} + \overline{\dot{\omega}_C} \tag{3.3}$$

$$\frac{\partial \overline{\rho_g} \tilde{u}_i}{\partial t} + \frac{\partial \overline{\rho_g} \tilde{u}_i \tilde{u}_j}{\partial x_j} = -\frac{\partial \overline{p}}{\partial x_i} + \frac{\partial (2\overline{\mu} \tilde{S}_{ij})}{\partial x_j} - \frac{\partial q_{ij}}{\partial x_j} + \overline{\dot{S}_i} \tag{3.4}$$

$$\tilde{\rho}_g = \tilde{\rho}_g(\tilde{Z}, \tilde{C}, \tilde{Z}") \tag{3.5}$$

$$\tilde{S}_{ij} = \frac{1}{2}(\frac{\partial \tilde{u}_i}{\partial u_j} + \frac{\partial \tilde{u}_j}{\partial u_i}) - \frac{1}{3}\delta_{ij}\frac{\partial \tilde{u}_k}{\partial x_k} \tag{3.6}$$

where the unclosed transport terms in the momentum and scalar equations are grouped into the residual stress q_{ij}, and residual scalar flux q_{Zj} and q_{Cj}. The dynamic Smagorinsky

model by Moin *et al.* (1991) is used to close these subgrid terms as demonstrated by Pierce & Moin (2001). For a two-fluid (air + fuel) mixture, one conserved scalar (the mixture fraction, Z) and a non-conserved scalar (the progress variable, C) are solved. The gas-phase properties such specific heat, molecular weight, density, viscosity, heat-release, and source terms in the progress-variable equation, $\overline{\dot{\omega}}_C$, are obtained from lookup tables generated using flamelet theory for non-premixed combustion and are dependent on the local values of Z, C, and the subgrid mixture fraction fluctuations, Z''.

With the presence of the liquid phase and inter-phase mass, momentum, and energy transport, additional source terms are added into the continuity, scalar transport and momentum equations. As the droplets evaporate the heat of vaporization is taken from the gas-phase and there is evaporative cooling of the surrounding gas. This gives rise to a sink term in the energy equation. By assuming adiabatic walls and unity Lewis number, the energy and scalar equations have the same boundary conditions and are linearly dependent. Only one scalar equation (for mixture fraction, Z) is solved and other scalars including temperature are deduced using flamelet tables. The evaporative cooling effect (heat of vaporization) is accounted for in the equation of state during the generation of the flamelet tables. The heat content of the liquid fuel is taken into account by computing an effective gaseous fuel enthalpy and is used in solving the flamelet equations.

3.2. *Modeling Primary Breakup/Dense Regime*

The initial breakup of the turbulent liquid film into large coherent structures is called primary breakup. It is dominated by the interaction of the turbulent liquid film with the surrounding turbulent gas-phase giving rise to liquid surface instability waves. These interfacial instabilities are important in the overall spray evolution and droplet formation process. However, the dynamics of the phase interface is highly complex and as of today not well understood. It in fact remains one of the outstanding unresolved problems in the area of spray simulation how to model this initial breakup in turbulent environments correctly. The majority of the atomization modeling effort is based on Lagrangian particle tracking and secondary breakup mechanisms as described later. Implicit in these models are the assumptions that a) the characteristic length scale of the liquid, ℓ, is small compared to the grid size, Δx, and b) the liquid volume fraction Θ_p is small. Although these models are successful in predicting secondary breakup in the 'intermediate' and 'dilute' regimes, they are not applicable in the 'primary breakup' and 'dense' regime, because their basic assumptions are invalid.

Two different but in essence complementary approaches are being pursued within the group to correctly predict the 'primary breakup' and 'dense' regime. On the one hand, a novel Eulerian based Large Surface Structure model is being developed that explicitly tracks the larger scale dynamics of the phase interface, $\ell/\Delta x > 1$. On the other hand, Lagrangian spray models are being extended to the 'dense regime' by accounting for drop/particle sizes that are comparable to but still smaller than the grid size, $\ell/\Delta x < 1$.

3.2.1. *Large Surface Structure Model*

The objective of the Large Surface Structure (LSS) Model is to correctly capture the dynamics of the phase interface in the primary breakup regime. To this end, we propose to follow in principle the LES approach for turbulent flows. All interface dynamics occurring on scales larger than the grid size are explicitly resolved and captured by a Eulerian level set approach, whereas interface dynamics occurring on the subgrid scales are described by an appropriate subgrid model. Details of this model and some preliminary test cases and results are given in a separate paper in this annual research brief (Herrmann 2003).

3.2.2. *Modeling Finite-Size Droplets*

In a parallel effort, the Lagrangian framework is extended to account for drop/particle sizes that are comparable to but still smaller than the grid size, $\ell/\Delta x < 1$. The equations are based on the original spray formulation developed by Dukowicz (1980) which consists of Eulerian fluid and Lagrangian particle calculations, and accounts for the displacement of the fluid by the particles as well as the momentum interchange between them. The gas-phase equations given above are modified to take into account the volume fraction ($\Theta = 1 - \Theta_p$), where Θ_p represents the volume occupied by the liquid-phase in a given control volume. The gas-phase density, ρ_g and pressure p are then replaced by ($\rho_g\Theta$) and ($p\Theta$) in the gas-phase governing equations.

In brief, the Lagrangian particles are advanced using Lagrangian particle tracking. The particle volume fraction Θ_p is then computed on each grid point and then the gas-phase equations are advanced. Use of volume fraction, however, adds to numerical complexity and accurate numerical schemes conserving liquid mass are being developed. Apte *et al.* (2003c) summarize the theoretical formulation and present some preliminary test cases in particulate flows.

3.3. *Modeling Intermediate Regime*

The particle motion is simulated using the Basset-Boussinesq-Oseen (BBO) equations (Crowe *et al.* 1998). It is assumed that the density of the particle is much larger than that of the fluid ($\rho_p/\rho_g \sim 10^3$), particle-size is small compared to the turbulence integral length scale, and that the effect of shear on particle motion is negligible. The high value of density ratio implies that the Basset force and the added mass term are small and are therefore neglected. Under these assumptions, the Lagrangian equations governing the droplet motions become

$$\frac{d\mathbf{x}_p}{dt} = \mathbf{u}_p, \tag{3.7}$$

$$\frac{d\mathbf{u}_p}{dt} = D_p \left(\mathbf{u} - \mathbf{u}_p\right) + \left(1 - \frac{\rho_g}{\rho_p}\right)\mathbf{g} \tag{3.8}$$

where m_p is the mass of the droplet, $\mathbf{u}_p$ the particle velocity components, $\mathbf{u}$ gas-phase velocities interpolated to the particle location, ρ_p and ρ_g the particle and gas-phase densities, and $\mathbf{g}$ the gravitational acceleration. The drag force on a solid particle is modeled using a drag-coefficient, C_d,

$$D_{p\,solid} = \frac{3}{4}C_d\frac{\rho_g}{\rho_p}\frac{|\mathbf{u}_g - \mathbf{u}_p|}{d_p} \tag{3.9}$$

where C_d is obtained from the nonlinear correlation (Crowe *et al.* 1998)

$$C_d = \frac{24}{Re}\left(1 + aRe_p^b\right). \tag{3.10}$$

Here $Re_p = d_p|\mathbf{u}_g - \mathbf{u}_p|/\mu_g$ is the particle Reynolds number. The above correlation is applicable for $Re_p \le 800$. The constants $a = 0.15, b = 0.687$ yield the drag within 5% from the standard drag curve. Modifications to the solid particle drag are applied to compute drag on a liquid drop and are given below.

3.4. *Deformation and Drag Models*

In order to quantify the effect of droplet deformation on drag, Helenbrook & Edwards (2002) performed detailed resolved simulations of axisymmetric liquid drops in uniform gaseous stream. The simulations were performed using an *hp*-finite element method (Helenbrook 2002). An unstructured mesh of triangles which deforms with the interface along with a dynamic mesh adaptation algorithm was used allowing higher-order accuracy to be obtained even though there is a discontinuity at the interface. This gives results for the drag which are accurate to within 1%. Based on their computations for a range of density and viscosity ratios, range of Weber (We), Ohnesorge (Oh), and Reynolds numbers (Re), a correlation was developed that provides the amount of deformation in the form of ellipticity, E, which is defined as the ratio of the height to width of the drop. This is given as,

$$E = 1 - 0.11We^{0.82} + 0.013\sqrt{\frac{\rho_l}{\rho_g}}\frac{\mu_g}{\mu_l}Oh^{-0.55}We^{1.1} \qquad (3.11)$$

where μ_l, μ_g are the viscosities of the liquid and gas and ρ_l, ρ_g are the densities, respectively. The non-dimensional Weber and Ohnesorge numbers are defined as, $We = \rho_g U^2 d_p/\sigma$ and $Oh = \mu_l/\sqrt{\rho_l\sigma d_p}$, where U is the relative velocity between the gas and liquid, d_p the diameter of the droplet, and σ the surface tension. Accordingly, $E < 1$ indicates that the drops have more width than height with deformation in the direction perpendicular to the relative velocity. These shapes are called oblate shapes. Similarly, $E > 1$ gives elongation in the direction of the relative velocity giving rise to prolate shapes. $E = 1$ implies spherical shapes.

The effect of droplet deformation is to change the drag force. This effect is modeled by using an effective equatorial droplet diameter, $d_p^* = d_p E^{-1/3}$. The particle Reynolds number is also modified, $Re_p^* = Re_p E^{-1/3}$ (Helenbrook & Edwards 2002). This is used in equations (3.9, 3.10) to obtain the modified drag. In addition the effect of internal circulation is modeled by changing the drag on a solid sphere as

$$\frac{D_{drop}}{D_{solid}} = \left(\frac{2 + 3\mu_l/\mu_g}{3 + 3\mu_l/\mu_g}\right)\left(1 - 0.03(\mu_g/\mu_l)Re_p^{0.65}\right) \qquad (3.12)$$

3.5. *Stochastic Model for Secondary Breakup*

Performing simulations of primary atomization where one tracks the liquid-gas interface in realistic combustor geometries is computationally intensive. Development of numerical techniques based on hybrid Eulerian/Lagrangian Level-set/Particle tracking schemes to capture the primary atomization process is ongoing and will be implemented into CDP. However, the current status is to compute the atomization process using advanced stochastic secondary breakup models developed (Apte *et al.* 2003). Emphasis is placed on obtaining the correct spray evolution characteristics such as liquid mass flux, spray angle, and droplet size distribution. The liquid film is approximated by large drops with size equal to the nozzle diameter and undergoes deformation and breakup. The effect of high mass-loading on the gas-phase momentum transport is captured through two-way coupling between the two phases.

In this model, the characteristic radius of droplets is assumed to be a time-dependent stochastic variable with a given initial size-distribution. The breakup of parent blobs into secondary droplets is viewed as the temporal and spatial evolution of this distribution function around the parent-droplet size according to the Fokker-Planck (FP) differen-

tial equation. This distribution function follows a certain long-time behavior, which is characterized by the dominant mechanism of breakup:

$$\frac{\partial T(x,t)}{\partial t} + \nu(\xi)\frac{\partial T(x,t)}{\partial x} = \frac{1}{2}\nu(\xi^2)\frac{\partial^2 T(x,t)}{\partial x^2}. \tag{3.13}$$

where the breakup frequency (ν) and time (t) are introduced. Here, $T(x,t)$ is the distribution function for $x = \log(r_j)$, and r_j is the droplet radius. Breakup occurs when $t > t_{breakup} = 1/\nu$. The value of the breakup frequency and the critical radius of breakup are obtained by the balance between the aerodynamic and surface tension forces. The secondary droplets are sampled from the analytical solution of equation (3.13) corresponding to the breakup time-scale. The parameters encountered in the FP equation ($\langle\xi\rangle$ and $\langle\xi^2\rangle$) are computed by relating them to the local Weber number for the parent blob, thereby accounting for the capillary forces and turbulent properties. As new droplets are formed, parent droplets are destroyed and Lagrangian tracking in the physical space is continued till further breakup events.

3.6. *Modeling Dilute Regime*

Typical spray simulations do not resolve the temperature and species gradients around each droplet to compute the rate of evaporation. Instead, evaporation rates are estimated based on quasi-steady analysis of a single isolated drop in a quiescent environment (Faeth 1977, Faeth 1983). Multiplicative factors are then applied to consider the convective and internal circulation effects. We model the droplet evaporation based on a 'uniform-state' model. The Lagrangian equations governing particle mass and heat transfer processes are well summarized by Oefelein (1997) and are described in brief.

$$\frac{d}{dt}(m_p) = -\dot{m}_p \tag{3.14}$$

$$m_p C_{pl}\frac{d}{dt}(T_p) = h_p \pi d_p^2(T_g - T_p) - \dot{m}_p \Delta h_v \tag{3.15}$$

where Δh_v is the latent heat of vaporization, m_p mass of the droplet, T_p temperature of the droplet, and C_{pl} the specific heat of liquid. The diameter of the droplet is obtained from its mass, $d_p = (6m_p/\pi\rho_p)^{1/3}$. h_p is the effective heat-transfer coefficient and is defined as

$$h_p = k_s\left(\frac{dT}{dr}\right)_{sg} / (T_g - T_s) \tag{3.16}$$

where k_s is the effective conductivity of the surrounding gas at the droplet surface. The subscript 's' stands for the surface of the droplet. The solutions to the mass and temperature equations for quiescent medium are obtained by defining Spalding mass and heat transfer numbers and making use of the Clausius-Clapeyron's equilibrium vapor-pressure relationship (Faeth 1977). In addition, several convective correction factors are applied to obtain spray evaporation rates at high Reynolds numbers (Faeth 1977, Faeth 1983).

3.7. *Hybrid Particle-Parcel Technique for Spray Simulations*

Performing spray breakup computations using Lagrangian tracking of each individual droplet gives rise to a large number of droplets ($\approx$ 10-30 million) very close to the injec-

tor. For LES, simulating all droplet trajectories would be ideal, however, this gives rise to severe load-balancing problems on parallel processors. We have developed a hybrid particle-parcel scheme to effectively reduce the number of particles tracked. A parcel or computational particle represents a group of droplets, N_{par}, with similar characteristics (diameter, velocity, temperature). During injection, new particles added to the computational domain are pure drops ($N_{par} = 1$). These drops move downstream and undergo breakup according to the secondary breakup model and produce new droplets.

The basic idea behind the hybrid-approach, is to collect all droplets in a particular control volume and group them into bins corresponding to their size and other properties such as velocity, temperature etc. The droplets in bins are then used to form a parcel by conserving mass, momentum and energy. The properties of the parcel are obtained by mass-weighted averaging from individual droplets in the bin. For this procedure, only those control volumes are considered for which the number of droplets increases above a certain threshold value. The number of parcels created would depend on the number of bins and the threshold value used to sample them. The parcel thus created then undergoes breakup according to the above stochastic sub-grid model, however, does not create new parcels. On the other hand, N_{par} is increased and the diameter is decreased by mass-conservation. This strategy reduces the total number of computational particles in the domain. In a real simulation with breakup and evaporation models, all the particles are clustered in a very small region close to the injector. This may still give rise to load-imbalance as only a few processors would solve the Lagrangian particle equations. Domain decomposition methods taking into account this load imbalance are being developed and will be tested in the present large-scale multi-physics simulation.

4. Validation Studies using CDP

A systematic and extensive validation effort of CDP code and the Lagrangian spray modules was initiated earlier and several simulations were performed to compare the LES predictions of gas and liquid/solid phases with the available experimental data. Apte *et al.* (2003a) first performed an LES of particle-laden swirling, co-annular jet and compared the results with the experiments of Sommerfeld & Qiu (1991). This validated the Lagrangian particle tracking scheme as well as the accuracy of the numerical method in swirling flows. In addition, development & validation of the secondary breakup model in simplified combustor geometries was also completed (Apte *et al.* 2003). This spray model validation effort was continued and applied to study model predictions for spray evaporation and breakup in complex geometries.

4.1. *Validation of Spray Breakup Model in PW Frontend Geometry*

The stochastic model along with the hybrid particle-parcel approach were used to simulate spray evolution from the Pratt and Whitney injector nozzle. Figure 8 shows the instantaneous snapshot of the spray field along with the injector geometry. The experimental data set was obtained by mounting the injector in a cylindrical plenum through which gas with prescribed mass-flow rate was injected. The gas goes through the main and guide swirler to create a swirling jet into the atmosphere. Liquid film is injected through the filmer surface which forms an annular ring. The liquid mass-flow rate corresponds to certain operating conditions of the gas-turbine engine. For this case, 3.2M grid points were used with high resolution near the injector. The domain decomposition is based on the optimal performance of the Eulerian gas-phase solver on 96 processors. Due to breakup, a large number of droplets are created in the vicinity of the injector. With
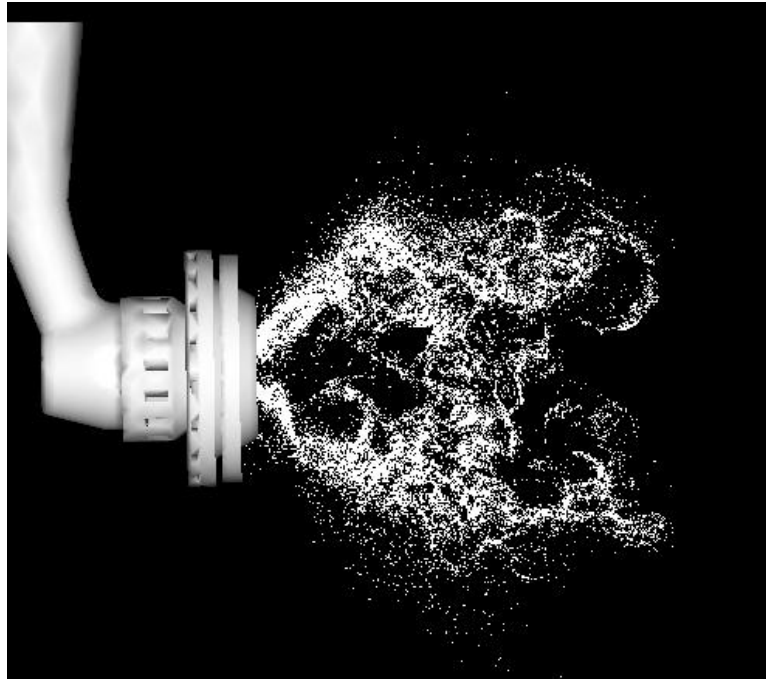
FIGURE 8. Spray evolution from a realistic gas-turbine injector: scatter plot shows the instantaneous droplet locations in $z = 0$ plane. Large size droplets are injected from the nozzle wall in an annular ring to form a hollow cone spray.
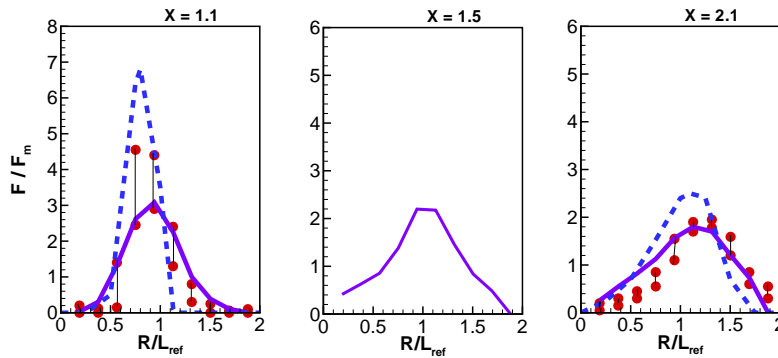

FIGURE 9. Comparison of radial variation of liquid axial mass flux at various axial locations, - - - - P&W RANS with TAB model , ——— present LES with stochastic model, ∘ — ∘ experimental error bar.

the hybrid approach, the total number of computational particles tracked at stationary state is around 3.5M, which represents approximately 13M droplets. This includes around 150,000 parcels. The load-imbalance due to atomization was found to be significant as only $1/3^{rd}$ of the processors had more than 10,000 computational particles. We are looking into advanced load-balancing techniques to reduce this computational overhead due to sprays. CDP-(α) has the capability of dynamic load-balancing based on particle imbalance as shown earlier. This will be used to perform these simulations to
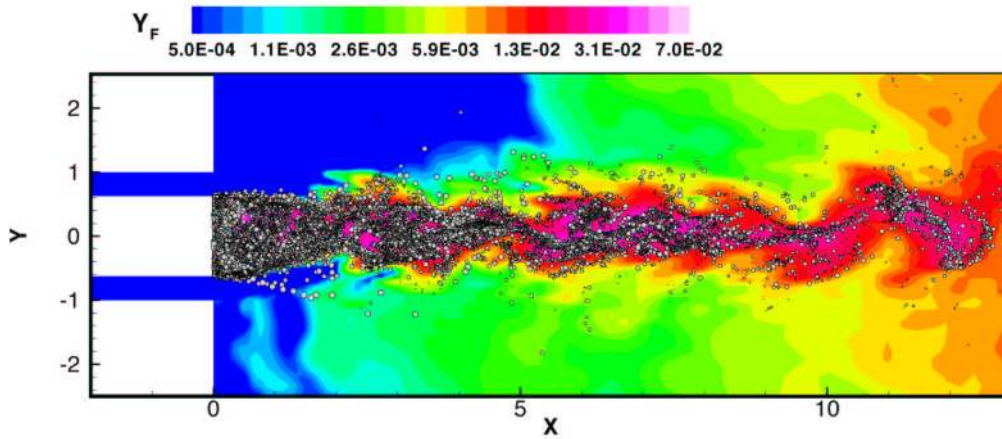
FIGURE 10. Instantaneous contours of ISO-propyl mass-fraction superimposed by droplet locations in $z = 0$ plane.

significantly improve the efficiency and speedup. It will also facilitate us to investigate advanced collision/coalescence models.

Figure (9) shows comparisons with the experimental data of radial variation of liquid mass-flowrates using LES with stochastic model for secondary breakup. Also shown are the predictions made by Pratt & Whitney's RANS-based simulation with a Taylor-Analogy Breakup (TAB) model. The LES results are generally in good agreement with the experiments. The liquid mass-flowrates basically relate to the spray angle and droplet size distributions obtained after breakup. The Sauter Mean Diameter (SMD) are well captured by the present LES simulation (within 7% of the experimental data). The diameter distributions when compared with the experimental data indicates a broad size-distribution as opposed to the one predicted by RANS with the TAB model. The size distribution also indicates presence of large number of small size droplets which could be attributed to the lack of models addressing droplet collision and coalescence. In addition, the initial droplet size at the injector nozzle is assumed to be constant in these simulations, whereas it may vary depending on the local conditions governing primary atomization. A further investigation with inclusion of collision models as well as using a size distribution at the inlet should be performed in order to accurately predict the spray characteristics.

4.2. *Validation of Spray Evaporation Model*

In order to validate the evaporation model and the variable density formulation in CDP, simulation of a coaxial non-swirling jet was performed following the configuration used in the experiments by Sommerfeld & Qiu (1998). This flow configuration was chosen because of its direct relevance in gas-turbine combustion chambers. In addition, in these experiments the boundary conditions for the liquid phase specifying the inlet droplet size distribution and their correlation with droplet velocity is well-defined. The gas-phase temperatures are not high enough to produce spray flames. This isolates the droplet evaporation problem from spray breakup and combustion and is very useful in validating the evaporation models used in CDP. Accordingly, only one scalar equation (mixture fraction) is solved and the gas-phase temperature is obtained from the ideal gas law.

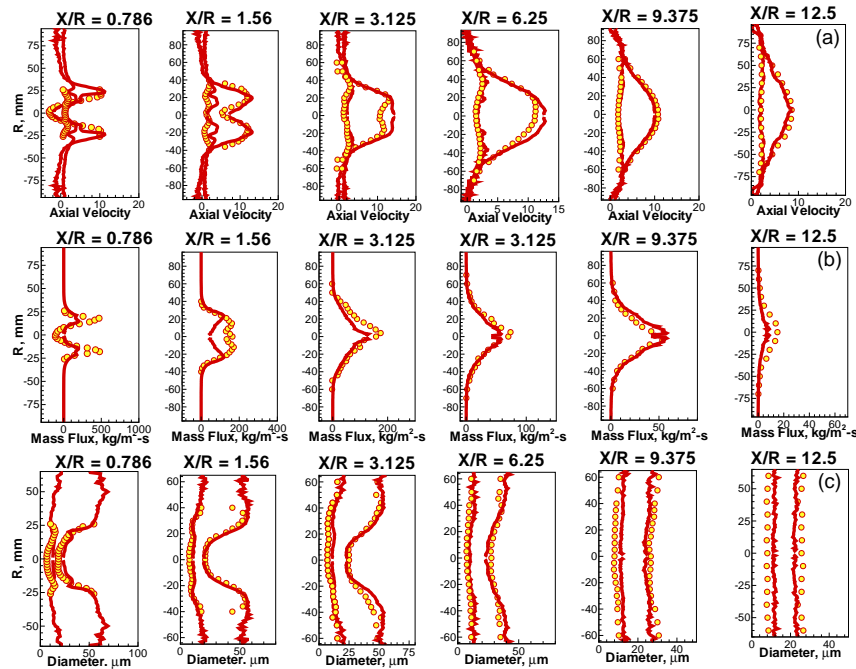The selection of droplet size and velocity at the injection surface is based on the given

FIGURE 11. Comparison of radial variation of evaporation statistics at various axial locations with the experimental data of Sommerfeld & Qiu (1998), ——— LES, ○ experimental data: a) mean and *rms* of axial particle velocity, b) mean axial liquid mass flux, c) mean and *rms* of particle droplet diameter.

experimental PDF of size-velocity correlations. The grid used consists of 1.5M hexahedral cells and around 0.5M particles were present in the computational domain at stationary state. Figure (10) shows a snapshot of mixture fraction contours superimposed by scatter plot of ISO-propyl alcohol particles in a coaxial combustor. The droplets are injected near the inlet circular wall of cross-sectional diameter 40 mm. The droplet velocity-size correlation depicts a conical spray with a spray angle of around 60^0. Figure (11) shows the droplet statistics. The radial variations of mean and *rms* droplet velocity, mean axial mass flux, and mean and *rms* droplet diameter compared with experimental data of Sommerfeld & Qiu (1998) are shown. The profiles are in good agreement with the experimental data. The droplet mean diameter profile is typical of the hollow cone atomizer, where smaller droplets are found in the core region and larger droplets near the edge of the spray. Away from the inlet section, the droplet mean diameter distribution becomes more uniform over the cross-section and slowly decreases in the downstream direction because of evaporation. The axial mass-flux also decreases towards the exit due to evaporation and is well captured by the present simulation. At $x = 0$ and $x = 0.786$ the profiles of droplet mass flux show two-peaks associated to hollow-cone spray. Due to the recirculation region downstream of the center-body, the droplet mass-flux becomes negative. Further downstream spreading of the spray is hindered by the annular air-jets and maximum of the mass flux moves towards the centerline. These features are well captured by the present LES computation.

5. Large Scale Multi-physics Simulation using CDP

A multi-scale, multi-physics simulation of turbulent reacting flow in a realistic Pratt & Whitney combustor was initiated. This simulation includes all the complex models for spray breakup, evaporation, and turbulent combustion described in section(3). This simulation will serve as the first validation study of the reacting multiphase flow solver (CDP) in complex combustor geometry. Figure (12) shows the combustor geometry in the symmetry plane $z = 0$. The simulation is performed for a single injector which represents one sector of the full combustor containing 18 injectors. Liquid fuel (Jet-A) enters the combustion chamber through an annular ring at the injector exit. This liquid film is approximated by large drops of the size of the annulus radius. These drops are convected by the surrounding hot air, they break, evaporate, and the fuel vapor thus formed mixes with the surrounding air giving a non-premixed spray flame. The computational grid consists of 1.9M hybrid elements (hexes, pyramids, and tets) with fine resolution close to the injector.

The flamelet library for Jet-A fuel at gas-turbine engine operating conditions, was generated by using a surrogate fuel of 80% n-Decane and 20% 1-2-4 tri-methyl-benzene which closely follows the chemical kinetics and reaction rates of the Jet-A fuel. Around 1000 elementary reactions among 100 chemical species were used to generate these tables. The chemical kinetics of surrogate fuel was compared with original fuel in terms of prediction of pollutants in laminar flames and showed good agreement. In this multiphase simulation, the flamelet tables are generated by considering the heat of vaporization of the liquid fuel. This is obtained by using heat-content for an equivalent gaseous fuel which gives large densities in the pure fuel-vapor region ($Z = 1$).

Figure (12) shows instantaneous snapshots of progress variable (C), mixture fraction (Z), normalized temperature (T/T_0), and velocity magnitude (u_{mag}) in the $z = 0$ symmetry plane. Scatter plot of droplets forming a conical spray is also shown. A highly complex unsteady flame is observed in this simulation. High temperatures in the combustion chamber are reduced by large mass-influx through the dilution holes. This reduces the exit temperature considerably. Strong recirculation zone with conical spray flame is observed near the nozzle. The droplets evaporate completely close to injector and do not appear beyond ($x = 2$). The experimental data available for validation includes pressure drops across different components, mass-splits through the inner and outer dilution holes, and swirlers. The comparison of these quantities with the experimental data was shown to be within 10% for the cold flow simulation. Similar results are obtained for the reacting flow case. In addition, the exit plane temperature was measured at 5 locations. The temperature field is within 10-15% of the experimental data near the center. The predicted temperature near the walls is much lower and is still evolving with time indicating that the flow has not reached the statistically stationary state.

This computation was performed on 80 processors on Frost and involved around 0.5M computational particles. The algebraic multigrid solver (AMG) developed at Lawrence Livermore is used to solve the Poisson equation. The convergence rate of the AMG solver was compared with the conjugate gradient solver (PCG). For each time-step, the conjugate gradient solver typically requires 2000 iterations, whereas the AMG solver requires 10-12 cycles corresponding to 500-600 conjugate gradient iterations. The AMG-solver gave an overall speed-up of 2-3 times over the PCG solver and reduced the computational time substantially.

6. Summary

CDP is the flagship LES code developed by the combustor group to perform LES of reacting multiphase flow in complex geometry. CDP is named after the late Charles David Pierce (1969-2002) who made several lasting contributions to the LES of reacting flows and to the DOE's ASCI program. CDP is a parallel unstructured finite-volume code developed specifically for LES of variable density low Mach-number flows. It is written in Fortran 90, uses MPI, and has integrated combustion and spray modules. A wide range of simulations of multiphase, reacting turbulent flows have been performed using CDP. It has been shown that the predictive capability of CDP for complex flows in realistic gas-turbine configurations is good. A major redesign and rewrite of CDP has been initiated to improve and add to the current capabilities. In the past year, major accomplishments included the following milestones:

• Multi-physics simulation in complex geometry: The first multi-physics simulation including fuel spray breakup, coalescence, evaporation, and combustion is being performed in a single periodic sector ($1/18^{th}$) of an actual Pratt & Whitney combustor geometry.

• Large scale simulation: Performed large eddy simulations of the complete combustor geometry (all 18 injectors) with over 100 million control volumes using CDP-α.

Further development of CDP-α will include the implementation of advanced combustion and primary atomization models, and modification of the numerical algorithm to capture acoustic waves and combustion instabilities based on the compressible formulation of Wall *et al.* (2002). Several large-scale, multiphysics simulations in the PW combustor using one or more sectors will be performed to assess the accuracy of the overall formulation.

7. Acknowledegement

REFERENCES

APTE, S. V., MAHESH, K., MOIN, P. & OEFELEIN, J.C. 2003a Large-eddy simulation of swirling particle-laden flows in a coaxial-jet combustor. *Int. J. Mult. Flow* **29**, 1311-1331.

APTE, S. V., GOROKHOVSKI, M. & MOIN, P. 2003b LES of atomizing spray with stochastic modeling of secondary breakup. *Int. J. Mult. Flow* **29**, 1503-1522.

APTE, S. V., MAHESH, K. & LUNDGREN, T. 2003c An Eulerian-Lagrangian model to simulate two-phase/particulate flows. *Annual Research Briefs*, 2003, Center for Turbulence Research.

CROWE, C., SOMMERFELD, M. & TSUJI, Y. 1998 Multiphase Flows with Droplets and Particles, CRC Press, Boca Raton, FL.

DELLENBACK, P.A., METZGER D.E. & NEITZEL, G.P. 1988 Measurements in Turbulent Swirling Flow Through an Abrupt Axisymmetric Expansion, *AIAA Journal*, **26**.

DUKOWICZ, J. K. 1980 A particle-fluid numerical model for liquid sprays. *J. Comput. Phys.* **35**, 229-253.

FAETH, G. 1977 Current status of droplet and liquid combustion. *Prog. Energy Combust. Sci.*, **3**: 191-224.

FAETH, G. 1983 Evaporation and combustion of sprays. *Prog. Energy Combust. Sci.*, **9**: 1-76.

HELENBROOK, B. T. 2002 A two-fluid spectral element method. *Comp. Meth. Appl. Mech. Eng.*, **191**, 273-294.

FALGOUT, R. D. AND YANG, U. M., "hypre: a Library of High Performance Preconditioners," in Computational Science - ICCS 2002 Part III, P.M.A. Sloot, C.J.K. Tan. J.J. Dongarra, and A.G. Hoekstra, Eds., Lecture Notes in Computer Science, **2331**, 632-641, 2002, Springer-Verlag. Also available as Lawrence Livermore National Laboratory technical report UCRL-JC-146175.

HELENBROOK, B. T. & EDWARDS, C. F. 2002 Quasi-steady Deformation and Drag of Uncontaminated Liquid Drops. *Int. J. Multi. Flows.*.

HERRMANN, M. 2003 Modeling primary breakup: A three-dimensional Eulerian level set/vortex sheet method for two-phase interface dynamics. *Annual Research Briefs*, Center for Turbulence Research, 2003.

MAHESH, K., CONSTANTINESCU, G. & MOIN, P. 2003 A new time-accurate finite-volume fractional-step algorithm for prediction of turbulent flows on unstructured hybrid meshes. *J. Comput. Phys.*, to appear.

MAVRIPLIS, D. J. & PIRZADEH, S. 1999 NASA/CR-1999-208999ICASE Report No. 99-9Large-scale Parallel Unstructured Mesh Computations for 3D High-lift Analysis.

MOIN, P., SQUIRES, K., CABOT, W. & LEE, S. 1991 A dynamic subgrid model for compressible turbulence and scalar transport. *Physics of Fluids. A.*, **3**, pp. 2746-2757.

OEFELEIN, J. C. 1997 Simulation and analysis of turbulent multiphase combustion processes at high pressures, Ph.D. Thesis, The Pennsylvania State University, University Park, Pa.

PARMETIS http://www-users.cs.umn.edu/ karypis/metis/parmetis/

PIERCE, C.D. & MOIN, P. 2001 Progress variable approach for large eddy simulation of turbulent combustion. *Report TF - 80*, Flow Physics and Computation Division, Mechanical Engineering Dept., Stanford University, Stanford, California.

SCHLUTER, J. & PITSCH, H. 2002 Consistent boundary conditions for integrated LES/RANS simulations: LES inflow conditions, *Annual Research Briefs*, Center for Turbulence Research.

SOMMERFELD, M. & QIU, H.H. 1991 Detailed measurements in a swirling particulate two -phase flow by a phase - Doppler anemometer. *Int. J. of Heat and Fluid Flow* **12**(1), 20-28.

SOMMERFELD, M. & QIU, H.H. 1998 Experimental studies of spray evaporation in turbulent flow. *Int. J. Heat & Fluid Flow* **19**, 10-22.

WALL, C., PIERCE, C. D. & MOIN, P. 2002 A semi-implicit method for resolution of acoustic waves in low mach number flows. *J. Comp. Phys.*, **181** (2), 545–563.
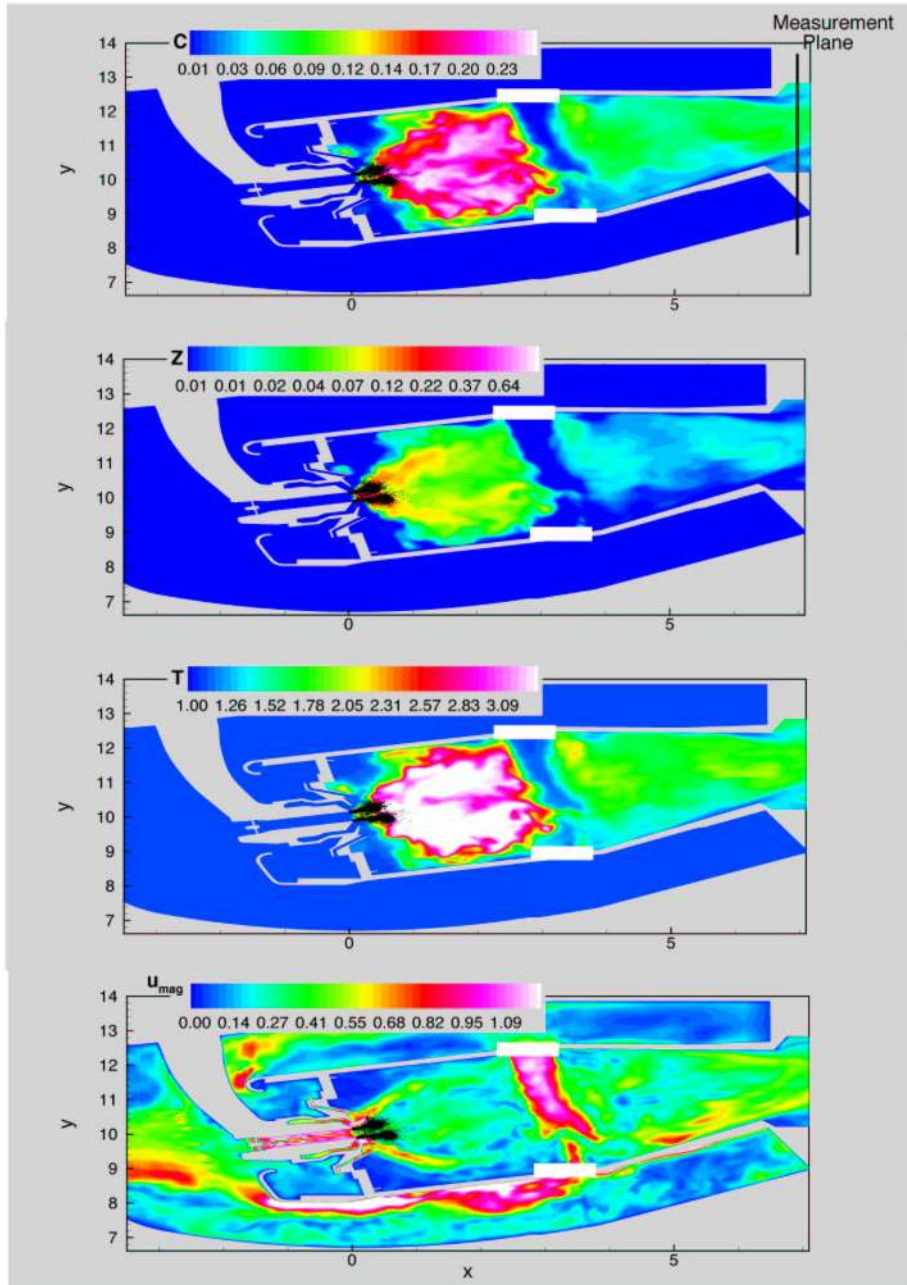
FIGURE 12. Instantaneous snapshots (from top to bottom) of progress variable, C, mixture fraction, Z, temperature normalized by inlet air temperature, T/T_0, and velocity magnitude, $\sqrt{u^2 + v^2 + w^2}$ superimposed with droplet scatter plot in Pratt & Whitney combustor, $z = 0$ plane. The geometry has been distorted.